Note from Eric: this Science paper contains the basic body of the text, 5 figures, and supplemental materials (you'll see a few references to the supplemental materials in the main text).

You won't need the supplemental materials to answer the questions on the cume, so those additional pages aren't included here.

Direct Imaging and Astrometric Discovery of a Superjovian Planet Orbiting an Accelerating Star

Thayne Currie, ^{1,2,3*} G. Mirek Brandt, ⁴ Timothy D. Brandt ⁴, Brianna Lacy ^{5,6}, Adam Burrows ⁵, Olivier Guyon ^{1,7,8}, Motohide Tamura ^{7,9,10}, Ranger Y. Liu ¹¹, Sabina Sagynbayeva ¹², Taylor Tobin ¹³, Jeffrey Chilcote ¹³, Tyler Groff ¹⁴, Christian Marois ^{15,16}, William Thompson ¹⁶, Simon Murphy ¹⁷, Masayuki Kuzuhara ⁷, Kellen Lawson ¹⁴, Julien Lozi ¹, Vincent Deo ¹, Sebastien Vievard ¹, Nour Skaf ¹, Taichi Uyama ¹⁸, Nemanja Jovanovic ¹⁹, Frantz Martinache ²⁰, N. Jeremy Kasdin ²¹, Tomoyuki Kudo ¹, Michael McElwain ¹⁴, Markus Janson ²², John Wisniewski ²³, Klaus Hodapp ²⁴, Jun Nishikawa ^{9,10}, Krzysztof Hełminiak ²⁵, Jungmi Kwon ¹⁰, Masa Hayashi ⁹

¹Subaru Telescope, National Astronomical Observatory of Japan, Hilo, HI, USA
 ²University of Texas-San Antonio, 1 UTSA Circle, San Antonio, TX, USA
 ³Eureka Scientific, Oakland, CA, USA

⁴Department of Physics, University of California, Santa Barbara, Santa Barbara, California, USA
 ⁵Department of Astrophysical Sciences, Princeton University, Princeton, NJ, USA
 ⁶Department of Astronomy, University of Texas-Austin, Austin, TX, USA
 ⁷Astrobiology Center, 2-21-1, Osawa, Mitaka, Tokyo, 181-8588, Japan
 ⁸Steward Observatory, The University of Arizona, Tucson, AZ 85721, USA
 ⁹National Astronomical Observatory of Japan, 2-21-2, Osawa, Mitaka, Tokyo, Japan
 ¹⁰Department of Astronomy, Graduate School of Science, The University of Tokyo, Tokyo, Japan
 ¹¹Parsons School of Design, New York, NY, USA

Department of Physics and Astronomy, State University of New York-Stony Brook, Stony Brook, NY, USA
 Department of Physics, University of Notre Dame, Notre Dame, IN, USA
 NASA-Goddard Space Flight Center, Greenbelt, MD, USA

¹⁵NRC-Herzberg, Victoria, BC, Canada

¹⁶Department of Physics and Astronomy, University of Victoria, Victoria, BC, Canada
 ¹⁷Centre for Astrophysics, University of Southern Queensland, Toowoomba, QLD 4350, Australia
 ¹⁸Infrared Processing and Analysis Center, California Institute of Technology, Pasadena, CA, USA
 ¹⁹Department of Astronomy, California Institute of Technology, Pasadena, CA, USA

²⁰Universite Cote d'Azur, Observatoire de la Cote d'Azur, CNRS, Laboratoire Lagrange, Nice, France

²¹Department of Mechanical Engineering, Princeton University, Princeton, NJ, USA
²²Department of Astronomy, Stockholm University, Stockholm, Sweden

²³Department of Physics and Astronomy, George Mason University, Fairfax, VA USA
²⁴Institute for Astronomy, University of Hawai i, Hilo, HI, USA

²⁵Nicolaus Copernicus Astronomical Center, Polish Academy of Sciences, Torun, Poland *To whom correspondence should be addressed; E-mail: currie@naoj.org.

Submitted to Science on February 18, 2022; Revised Version Passed Independent Peer Review on July 5, 2022

We detect a superjovian extrasolar planet around the dusty A star HIP 99770 using precision astrometry from the Gaia and Hipparcos satellites and direct imaging using the Subaru Coronagraphic Extreme Adaptive Optics Project. HIP 99770 b is the first exoplanet ever discovered jointly through direct imaging and precision astrometry and the first discovery leveraging on μ -arcsecond precision Gaia astrometry. HIP 99770 b is in a low-eccentricity orbit \sim 16.9 au from the primary, receiving about as much light as Jupiter does from the Sun. The planet induces an astrometric acceleration on the host star; its directly-measured companion-to-primary mass ratio is similar to that of many radial-velocity detected planets and some of the first imaged exoplanets, including HR 8799 cde. The planet's spectrum reveals an atmosphere resembling a slightly less cloudy and likely older analogue of these first imaging discoveries, enabling a new, critical probe of how gas giant planets evolve with time.

HIP 99770 b's discovery is a direct proof-of-concept for a fundamentally new strategy for finding imageable planets: selecting targets based on dynamical evidence from indirect methods like astrometry instead of conducting blind searches. This combined approach prefigures the campaigns that could one day directly detect and characterize an extrasolar Earth-like planet.

One sentence summary: HIP 99770 b is the first exoplanet jointly discovered through direct imaging and precision astrometry: a proof-of-concept for a fundamentally new approach for finding imageable exoplanets, including exo-Earths with future telescopes.

Introduction

Over the past 13 years, adaptive optics-assisted ground based telescopes have provided the first direct imaging discoveries of extrasolar planets (1-6), a key step towards imaging and characterizing the atmosphere of another Earth. These discoveries draw from *blind* surveys, where targets are selected based on system properties like age and distance. Unfortunately, the low yields of blind surveys show that currently imageable exoplanets are rare (7). Direct imaging provides exceptional constraints on exoplanet atmospheres (8). However, masses for imaged exoplanets are almost never directly measured but instead inferred through luminosity evolution models that are intrinsically uncertain and rely on difficult-to-constrain stellar ages (9, 10). The typically short time baselines and wide separations of imaged exoplanets can also leave orbital parameters derived purely from imaging highly uncertain (11).

Instead of conducting blind searches, coupling direct imaging searches with another indirect detection method can in principle radically improve discovery yields and simultaneously

explore the atmospheres, orbits, and masses for a large population of exoplanets. Astrometric monitoring can identify stars undergoing a proper motion acceleration caused by an unseen but imageable companion, including young stars unsuitable for precise RV measurements (12). Combining the imaged planet's relative astrometry with absolute astrometry of the star yields precise, directly-determined companion masses and improved constraints on orbital properties (12, 13). The micro-arcsecond precision of the European Space Agency's Gaia mission combined with measurements 20+ years prior from its predecessor, Hipparcos, makes possible the astrometric detection of superjovian planets at Jupiter-to-Neptune like separations around the nearest stars for the first time (14).

Target Properties and Data

HIP 99770 (HD 192640; 29 Cyg) is a chemically-peculiar A-type star with an effective temperature of \approx 8000 K, luminosity of \approx 13.9 L_{\odot} , and mass of \approx 1.7–2.0 M_{\odot} located \sim 40.74 pc from the Sun (Table 1). It is likely either \sim 40 Myr or 115–414 Myr old, depending on whether its kinematics or Hertzsprung-Russell (HR) diagram position is used to assess age. The star is surrounded by a luminous cold, Kuiper belt-like debris disk on > 150 au scales. See Supplemental Material for more details.

We searched for evidence that HIP 99770 shows an astrometric acceleration due to an unseen companion: a deviation from linear motion across the sky. We used astrometry from the Hipparcos-Gaia Catalogue of Accelerations (HGCA) (15), a cross-calibration of the Hipparcos and Gaia missions. HIP 99770's average proper motion—its position difference over the \approx 25 years between the Hipparcos and Gaia missions—differs from the proper motion measured around 2016 by Gaia EDR3 (16). HGCA yields $\chi^2 \sim 7.23$ for constant linear motion, revealing a significant acceleration (\approx 2.2 Gaussian sigma) with a false positive rate of 2.7%. The astrometric acceleration provides a lower limit to the ratio $M_{\rm sec}/R_{\rm sec}^2$, and suggests a \approx 11 $M_{\rm Jup}$ companion at a fiducial separation of 0".5 (\approx 20 au). Previous high-contrast imaging observations rule out a stellar/substellar companion at wide ($\rho > 1$ ") separations (see Supplemental Material), strongly hinting that HIP 99770's companion orbits closer in and has a lower mass.

We observed HIP 99770 with SCExAO coupled to the Coronagraphic High-Resolution Imager and Spectrograph (CHARIS), in low-resolution (broadband) mode in 22 spectral channels covering the major near-infrared (IR) passbands simultaneously ($\lambda = 1.16-2.37~\mu m$) (17, 18). Our first two data sets consisted of two shallow observing sequences in July and September 2020. Between May and October 2021, we conducted three deeper follow-up SCExAO/CHARIS observations and obtained one complementary data set in the thermal IR (L_p , $\lambda = 3.78~\mu m$) with the NIRC2 camera on the Keck II Telescope.

SCExAO/CHARIS reveals a faint point source, hereafter HIP 99770 b, located $\rho \sim 0.43$ "– 0.44" southeast of its host star (Figure 1; Table 1). In the highest-quality data, HIP 99770 b is visible across the entire spectral range using advanced PSF subtraction methods combined with different observing/residual noise suppression strategies (Figure 2, left panel). Each CHARIS

data set shows a clear detection, establishing an astrometric baseline longer than one year (middle panel). We also recover HIP 99770 b in Keck/NIRC2 thermal IR data (right panel).

Analysis

Our astrometry easily rejects HIP 99770 b being a background object at the >15- σ level. Between our first epoch (29 July 2020) and fourth epoch (13 July 2021), a background star should appear to move by \sim 65 mas to both the west and south (Table 1) due to the star's proper motion. However, over this time baseline HIP 99770 b moved 23 \pm 6 mas to the east and 29 \pm 6 mas to the north: i.e. in the *opposite* direction expected for a background star.

To determine HIP 99770 b's orbital properties and mass, we simultaneously fit its relative astrometry (from imaging data) and the primary's proper motions and anomalies (from the HGCA) using orvara (19). We adopted the standard uninformative priors discussed in (20), but use a more conservative uniform prior on the companion mass and a Gaussian $1.8 \pm 0.2 M_{\odot}$ prior on the primary. We performed additional tests adopting a $1/M_{\rm p}$ companion prior and changing the prior for the primary mass (see Supplemental Material); these changes have little effect on our results.

The posterior distributions from orvara for HIP 99770 b's orbital parameters constrain key properties (Figure 3). We derive a semimajor axis of $16.9^{+3.4}_{-1.9}$ au: comparable to HR 8799 e's orbit (21). HIP 99770 b's eccentricity is low, $e = 0.25^{+0.14}_{-0.16}$: more similar to values for directly imaged planets than brown dwarfs (11).

HIP 99770 b has a dynamical mass of $16.1^{+5.4}_{-5.0}$ $M_{\rm J}$, for a mass ratio of $q=(8.7\pm2.9)\times10^{-3}$. Adopting a $1/M_{\rm p}$ prior on the companion mass instead of a linear prior yields a mass of $13.9^{+6.1}_{-5.1}$ $M_{\rm J}$ ($q=(7.7\pm3.1)\times10^{-3}$). HIP 99770 b's mass is lower than the local minimum in values empirically separating massive planets from brown dwarfs (see Supplemental Material). HIP 99770 b's mass ratio is intermediate between mass ratios measured for some exoplanets like HR 8799 e ($q\approx6\times10^{-3}$) and those inferred for other, wider-separation exoplanets like TYC 8998-760-1 b ($q\approx0.01$ -0.015) but is much lower than mass ratios measured for the brown dwarfs GJ 758 B and HD 33632 Ab (q>0.04) (4,20-22).

Comparing HIP 99770 b's CHARIS spectrum to a library of substellar object spectra and spectral standards provides a first, coarse estimate of its temperature (23, 24). These comparisons show that HIP 99770 b lies at the critical transition from cloudy, methane poor L-type substellar objects to (nearly) cloud-free, T-type objects showing methane absorption (the "L/T transition"). The L7 field dwarf template best reproduces its spectrum amongst all spectral standards. In the spectral library, the L9.5 field dwarf SIMPJ0956-1447 best fits HIP 99770 b. Thus, we assign HIP 99770 b a spectral type of L7–L9.5, which corresponds to a likely effective temperature of $T_{\rm eff} \sim 1300-1500~K~(25)$. HIP 99770 b's atmosphere appears intermediate between SIMPJ0956-1447 and the directly imaged, extremely cloudy L/T transition exoplanet HR 8799 d (Figure 4, top panel).

We further characterize HIP 99770 b's atmosphere, comparing its CHARIS spectrum and

NIRC2 photometry to multiple grids of atmospheric models spanning a range of temperatures and gravities and adopting different prescriptions for clouds and atmospheric dust. Atmospheric models require clouds to match HIP 99770 b's spectrum, although the planet is likely less cloudy/dusty than the HR 8799 planets. The best-fitting models cover $\log(g) = 4$ –4.25 and temperature of 1450 K (Figure 4, bottom panel; Supplemental Material); well-fitting models have $\log(g) = 4$ –4.5 and temperatures of 1300–1500 K. HIP 99770 b's range of best-fitting temperatures and radii yield a luminosity of $\log(L/L_{\odot}) = -4.55 \pm 0.02$, or a luminosity ratio of 2×10^{-6} relative to the primary. Masses inferred from luminosity evolution are consistent with the planet's dynamical mass if the system is ~ 80 –200 Myr old (see Supplemental Materials).

The architecture of the HIP 99770 planetary system draws comparisons to the solar system. HIP 99770 b orbits at \sim 16.9 au, intermediate between the distances of Saturn and Uranus from the Sun. The system's cold debris disk is likely >150 au from the star, about 3.5 times the typical distance from the Sun to Kuiper belt objects. However, the insolation for HIP 99770 b is comparable to that at \sim 4.5 au in the solar system, very close to the orbit of Jupiter. Likewise, HIP 99770's debris disk, if at 150 au, lies at a luminosity-scaled distance comparable to that of the Kuiper belt from the Sun. Thus, like HR 8799, HIP 99770 bears some characteristics of a scaled-up version of our own solar system, albeit one where a single massive planet dominates.

The mass ratios (q) and separations (a_p) of substellar companions provide a coarse diagnostic of formation processes. Surveys suggest that the companion mass function for substellar objects reaches a local minimum at $q \sim 0.025$ where small (large) q values better probe planets formed in a disk (brown dwarf companions formed by fragmentation) (26). Stellar companions formed through fragmentation have q values as small as 0.08 (27). As with a few other RV-detected companions orbiting stars more massive than the Sun with masses at or slightly above the deuterium-burning limit, HIP 99770 b's mass ratio and separation ($q \sim 0.0087$, $a_p \sim 16.9$ au) is contiguous with planets below the deuterium-burning limit detected by both direct imaging and RV (Figure 5). Supplemental Material discusses the taxonomy of companions in more detail and shows why HIP 99770 b is also contiguous with the planet population, not brown dwarfs, in terms of mass.

Significance

HIP 99770 b is the first extrasolar planet jointly discovered through direct and indirect techniques: direct imaging and precision astrometry. HIP 99770 b joins β Pic bc and HR 8799 e as the only imaged planets with both spectra and dynamical masses. Analysis combining dynamics and luminosity evolution suggests that HIP 99770 b is older than these planets. A precise, directly-constrained age for the HIP 99770 primary – e.g. from future CHARA interferometry – will solidify HIP 99770 b as a critical benchmark for understanding planet atmospheric evolution.

HIP 99770 b also provides a potentially key test of direct imaging technologies. The *Roman Space Telescope* Coronagraphic Instrument (CGI) technological demonstration is a key stepping

stone to image an Earth-like planet with a future flagship mission and requires demonstrating a contrast deeper than 10^{-7} at $\lambda_c \leq 600$ nm (>10% bandpass) located 6–9 λ /D (~ 0.3 "–0.45") from a very bright ($V_{AB} \leq 5$) star. Current best-estimated performance predicts a contrast of $\sim 10^{-9}$ over this range. Our best-fit orbit places HIP 99770 b at [E,N]" = [0.358,-0.137] \pm [0.025,0.024], [0.354,-0.040] \pm [0.043,0.035], and [0.325,0.058] \pm [0.072,0.045] on dates covering CGI's likely performance period (July 1 2026, July 1 2028, and July 1 2030, respectively). We predict HIP 99770 b's contrast in CGI's band 1 centered on 575 nm to be 1.7×10^{-10} to 2.3×10^{-9} and depending primarily on clouds/atmospheric dust and surface gravity. For a subset of solutions, HIP 99770 b would be imageable by CGI at 575 nm and thus suitable for the CGI technological demonstration. At longer wavelengths (660 nm–730 nm), HIP 99770 b's contrast is milder ($\sim 10^{-8}$ – 10^{-7}) and should be detectable with CGI spectroscopy. Provided that CGI performs as expected, HIP 99770 could be an excellent test of ultra-deep contrasts from space and exoplanet spectroscopic characterization in the optical. See Supplemental Material for more details.

Finally, HIP 99770 b is a proof-of-concept a fundamentally different approach for finding imageable planets: conducting a *targeted*, dynamics-selected search for young Jupiters instead of a blind survey. Early results from our pilot accelerating star program suggest a discovery yield substantially higher than blind surveys conducted with comparably powerful instruments (28). The need to select imaging targets through either precision astrometry or extreme-precision RV will be potentially even more important for the efficient direct detection of short-period, Earth and Jupiter-like planets in reflected light on the ground with future facilities like the *Thirty Meter Telescope* or in space with the NASA direct imaging flagship mission endorsed by the Astro 2020 Decadal Survey or highlighted in the European Space Agency's Voyage 2050 report (29).

References

- 1. C. Marois, B. Zuckerman, Q. M. Konopacky, B. Macintosh, T. Barman, *Nature* **468**, 1080 (2010).
- 2. A.-M. Lagrange, et al., Science 329, 57 (2010).
- 3. J. Carson, et al., ApJL **763**, L32 (2013).
- 4. T. Currie, et al., ApJL **780**, L30 (2014).
- 5. B. Macintosh, et al., Science **350**, 64 (2015).
- 6. G. Chauvin, et al., A&A **605**, L9 (2017).
- 7. E. L. Nielsen, et al., AJ **158**, 13 (2019).
- 8. Q. M. Konopacky, T. S. Barman, B. A. Macintosh, C. Marois, *Science* **339**, 1398 (2013).

- 9. D. S. Spiegel, A. Burrows, *ApJ* **745**, 174 (2012).
- 10. M. Bonnefoy, et al., A&A 618, A63 (2018).
- 11. B. P. Bowler, S. C. Blunt, E. L. Nielsen, *AJ* **159**, 63 (2020).
- 12. T. D. Brandt, T. J. Dupuy, B. P. Bowler, *AJ* **158**, 140 (2019).
- 13. I. A. G. Snellen, A. G. A. Brown, *Nature Astronomy* **2**, 883 (2018).
- 14. M. Perryman, J. Hartman, G. Á. Bakos, L. Lindegren, *ApJ* **797**, 14 (2014).
- 15. T. D. Brandt, *ApJS* **254**, 42 (2021).
- 16. Gaia Collaboration, et al., A&A **649**, A1 (2021).
- 17. N. Jovanovic, et al., PASP 127, 890 (2015).
- 18. T. D. Groff, et al., Ground-based and Airborne Instrumentation for Astronomy VI (2016), vol. 9908 of Society of Photo-Optical Instrumentation Engineers (SPIE) Conference Series, p. 99080O.
- 19. T. D. Brandt, et al., AJ **162**, 186 (2021).
- 20. G. M. Brandt, et al., arXiv e-prints p. arXiv:2109.07525 (2021).
- 21. G. M. Brandt, T. D. Brandt, T. J. Dupuy, D. Michalik, G.-D. Marleau, *ApJL* **915**, L16 (2021).
- 22. A. J. Bohn, et al., ApJL 898, L16 (2020).
- 23. J. Gagné, D. Lafrenière, R. Doyon, L. Malo, É. Artigau, *ApJ* 783, 121 (2014).
- 24. K. L. Cruz, et al., AJ 155, 34 (2018).
- 25. D. C. Stephens, et al., ApJ 702, 154 (2009).
- 26. M. Reggiani, et al., A&A 586, A147 (2016).
- 27. M. Bonavita, et al., arXiv e-prints p. arXiv:2103.13706 (2021).
- 28. T. Currie, et al., Society of Photo-Optical Instrumentation Engineers (SPIE) Conference Series (2021), vol. 11823 of Society of Photo-Optical Instrumentation Engineers (SPIE) Conference Series, p. 1182304.
- 29. J. P. Greco, A. Burrows, ApJ 808, 172 (2015).
- 30. S. J. Murphy, E. Paunzen, *MNRAS* **466**, 546 (2017).

- 31. J. W. Jones, The ages of A-stars, Ph.D. thesis, Georgia State University, United States (2016).
- 32. F. Royer, J. Zorec, A. E. Gómez, *A&A* **463**, 671 (2007).
- 33. T. Currie, et al., ApJL **760**, L32 (2012).
- 34. C. Marois, D. Lafrenière, R. Doyon, B. Macintosh, D. Nadeau, ApJ 641, 556 (2006).
- 35. W. B. Sparks, H. C. Ford, ApJ 578, 543 (2002).
- 36. A. Z. Greenbaum, et al., AJ 155, 226 (2018).
- 37. A. Zurlo, et al., A&A 587, A57 (2016).
- 38. F. Allard, D. Homeier, B. Freytag, *Philosophical Transactions of the Royal Society of London Series A* **370**, 2765 (2012).
- 39. N. Madhusudhan, A. Burrows, T. Currie, *ApJ* **737**, 34 (2011).
- 40. G. T. van Belle, K. von Braun, ApJ **694**, 1085 (2009).
- 41. A. Slettebak, *ApJ* **115**, 575 (1952).
- 42. R. O. Gray, AJ 95, 220 (1988).
- 43. J. A. Cardelli, G. C. Clayton, J. S. Mathis, *ApJ* **345**, 245 (1989).
- 44. M. J. Pecaut, E. E. Mamajek, *ApJS* **208**, 9 (2013).
- 45. R. Lallement, B. Y. Welsh, J. L. Vergely, F. Crifo, D. Sfeir, *A&A* 411, 447 (2003).
- 46. W. Reis, W. Corradi, M. A. de Avillez, F. P. Santos, *ApJ* **734**, 8 (2011).
- 47. B. Zuckerman, J. H. Rhee, I. Song, M. S. Bessell, *ApJ* **732**, 61 (2011).
- 48. B. Zuckerman, *ApJ* **870**, 27 (2019).
- 49. Gaia Collaboration, et al., A&A 616, A10 (2018).
- 50. J. Jones, et al., ApJ 813, 58 (2015).
- 51. S. J. Murphy, M. Joyce, T. R. Bedding, T. R. White, M. Kama, MNRAS **502**, 1633 (2021).
- 52. T. R. Bedding, et al., Nature **581**, 147 (2020).
- 53. S. J. Murphy, et al., arXiv e-prints p. arXiv:2111.04203 (2021).
- 54. M. Asplund, N. Grevesse, A. J. Sauval, P. Scott, *ARA&A* 47, 481 (2009).

- 55. L. M. Rebull, et al., ApJ **681**, 1484 (2008).
- J. Milli, et al., Adaptive Optics Systems VI, L. M. Close, L. Schreiber, D. Schmidt, eds. (2018), vol. 10703 of Society of Photo-Optical Instrumentation Engineers (SPIE) Conference Series, p. 107032A.
- 57. T. Currie, et al., AJ **156**, 291 (2018).
- 58. T. Currie, et al., Society of Photo-Optical Instrumentation Engineers (SPIE) Conference Series (2020), vol. 11448 of Society of Photo-Optical Instrumentation Engineers (SPIE) Conference Series, p. 114487H.
- 59. C. Marois, R. Doyon, R. Racine, D. Nadeau, *PASP* **112**, 91 (2000).
- 60. N. Jovanovic, et al., The Astrophysical Journal Letters 813, L24 (2015).
- 61. T. D. Brandt, et al., Journal of Astronomical Telescopes, Instruments, and Systems 3, 048002 (2017).
- 62. T. Currie, et al., ApJ **729**, 128 (2011).
- 63. T. Currie, et al., ApJL 814, L27 (2015).
- 64. D. Lafrenière, C. Marois, R. Doyon, D. Nadeau, É. Artigau, *ApJ* **660**, 770 (2007).
- 65. C. Marois, B. Macintosh, J.-P. Véran, *Proc. SPIE* (2010), vol. 7736 of *Society of Photo-Optical Instrumentation Engineers (SPIE) Conference Series*, p. 77361J.
- 66. R. Soummer, L. Pueyo, J. Larkin, *ApJL* **755**, L28 (2012).
- 67. L. Pueyo, ApJ 824, 117 (2016).
- 68. E. L. Nielsen, et al., ApJ **750**, 53 (2012).
- 69. J. P. Greco, T. D. Brandt, *ApJ* **833**, 134 (2016).
- 70. R. Galicher, et al., A&A **594**, A63 (2016).
- 71. W. Thompson, C. Marois, *AJ* **161**, 236 (2021).
- 72. A. Burrows, D. Sudarsky, I. Hubeny, *ApJ* **640**, 1063 (2006).
- 73. J. Tennyson, et al., Journal of Molecular Spectroscopy 327, 73 (2016).
- 74. K. L. Chubb, et al., A&A **646**, A21 (2021).
- 75. E. Gharib-Nezhad, et al., ApJS **254**, 34 (2021).

- 76. N. F. Allard, F. Spiegelman, J. F. Kielkopf, *A&A* **589**, A21 (2016).
- 77. N. F. Allard, F. Spiegelman, T. Leininger, P. Molliere, *A&A* **628**, A120 (2019).
- 78. I. Hubeny, A. Burrows, *ApJ* **669**, 1248 (2007).
- 79. T. S. Barman, B. Macintosh, Q. M. Konopacky, C. Marois, *ApJL* **735**, L39 (2011).
- 80. I. Baraffe, G. Chabrier, T. S. Barman, F. Allard, P. H. Hauschildt, A&A 402, 701 (2003).
- 81. B. Lacy, A. Burrows, *ApJ* **892**, 151 (2020).
- 82. G. Gatewood, H. Eichhorn, *AJ* **78**, 769 (1973).
- 83. J. L. Bean, et al., ApJL 711, L19 (2010).
- 84. M. W. Muterspaugh, et al., AJ 140, 1657 (2010).
- 85. J. Sahlmann, et al., A&A 565, A20 (2014).
- 86. A. Venner, L. A. Pearce, A. Vanderburg, arXiv e-prints p. arXiv:2111.03676 (2021).
- 87. M. J. Pecaut, E. E. Mamajek, E. J. Bubar, *ApJ* **746**, 154 (2012).
- 88. E. E. Mamajek, C. P. M. Bell, *MNRAS* **445**, 2169 (2014).
- 89. T. J. Dupuy, et al., Research Notes of the American Astronomical Society 4, 54 (2020).
- 90. C. Marois, et al., Science **322**, 1348 (2008).
- 91. J. J. Wang, et al., AJ 156, 192 (2018).
- 92. J. Milli, et al., A&A 597, L2 (2017).
- 93. T. Currie, et al., ApJL 877, L3 (2019).
- 94. A. Niedzielski, G. Nowak, M. Adamów, A. Wolszczan, *ApJ* **707**, 768 (2009).
- 95. L. J. Rosenthal, et al., ApJS 255, 8 (2021).
- 96. K. Wagner, et al., ApJL 902, L6 (2020).
- 97. S. Hinkley, et al., ApJL 806, L9 (2015).
- 98. M. Kuzuhara, et al., ApJ 774, 11 (2013).
- 99. Q. M. Konopacky, et al., ApJL 829, L4 (2016).
- 100. D. S. Spiegel, A. Burrows, J. A. Milsom, *ApJ* **727**, 57 (2011).

- 101. K. M. Kratter, R. A. Murray-Clay, A. N. Youdin, *ApJ* **710**, 1375 (2010).
- 102. J. Sahlmann, et al., A&A **525**, A95 (2011).
- 103. G. Chabrier, et al., Protostars and Planets V, B. Reipurth, D. Jewitt, K. Keil, eds. (2007), p. 623.
- 104. K. L. Luhman, *Extreme Solar Systems*, D. Fischer, F. A. Rasio, S. E. Thorsett, A. Wolszczan, eds. (2008), vol. 398 of *Astronomical Society of the Pacific Conference Series*, p. 357.
- 105. K. Todorov, K. L. Luhman, K. K. McLeod, *ApJL* **714**, L84 (2010).
- 106. M. C. Liu, et al., ApJL 777, L20 (2013).
- 107. A. Quirrenbach, T. Trifonov, M. H. Lee, S. Reffert, A&A **624**, A18 (2019).
- 108. D. Grether, C. H. Lineweaver, *ApJ* **640**, 1051 (2006).
- 109. S. Udry, *In the Spirit of Lyot 2010*, A. Boccaletti, ed. (2010), p. E11.
- 110. F. Kiefer, et al., A&A **631**, A125 (2019).
- 111. S. M. Andrews, J. P. Williams, *ApJ* **659**, 705 (2007).
- 112. J. P. Williams, L. A. Cieza, *ARA&A* **49**, 67 (2011).
- 113. A. L. Kraus, M. J. Ireland, F. Martinache, J. P. Lloyd, *ApJ* **679**, 762 (2008).
- 114. T. J. Dupuy, M. C. Liu, *ApJS* **201**, 19 (2012).

Acknowledgments

We thank the Subaru Time Allocation committee, NASA-Keck Time Allocation Committee, and Subaru Director Michitoshi Yoshida for their support of this program through Open Use and Director's Discretionary Time allocations. This research is based on data collected at Subaru Telescope, which is operated by the National Astronomical Observatory of Japan. The authors acknowledge the very significant cultural role and reverence that the summit of Maunakea holds within the Hawaiian community. We are most fortunate to have the opportunity to conduct observations from this mountain. We thank Jonathan Gagne, Eric Mamajek, Richard Gray, and Jeremy Jones for extensive and helpful conversations regarding HIP 99770 A's spectral type, mass, and age. This work was partially funded under NASA/XRP program NNX17AF88G and NASA-Keck Principal Investigator Award (Program 2020A_N027). We acknowledge the support of the Natural Sciences and Engineering Research Council of Canada (NSERC). The development of SCExAO was supported by the Japan Society for the Promotion of Science

(Grant-in-Aid for Research #23340051, #26220704, #23103002, #19H00703 and #19H00695), the Astrobiology Center of the National Institutes of Natural Sciences, Japan, the Mt Cuba Foundation and the director's contingency fund at Subaru Telescope.

Table 1: HIP 99770 Planetary System Data

HIP 99770 A

Property		Value	References
$T_{ m eff}$		8000 K	$(30)^a$
Spectral Type		kA1.5hA7mA0.5 λ Boo (A5–A6)	$(30)^a$
Mass		$1.85\pm0.19~M_{\odot}$	(31), this work
Rotation Rate (Projected)		$65 \ km \ s^{-1}$	(32)
Apparent Luminosity		$13.86^{+2.14}_{-5.46} L_{\odot}$	this work
Age		40 Myr, 115-414 Myr	this work
Distance		$40.74 \pm 0.15 \ pc$	(16)
Proper Motion (Gaia-eDR3)		68.09 ± 0.12 , 69.40 ± 0.14 mas ${ m yr}^{-1}$	(15, 16)
Proper Motion (H-G scaled)		68.24 ± 0.01 , 69.67 ± 0.01 mas yr^{-1}	(15, 16)
Proper Motion (Hipparcos)		69.45 ± 0.38 , $69.19 \pm 0.38~{ m mas~yr^{-1}}$	(15, 16)
Proper Motion Anomaly (χ^2)		7.23	(15)
J,H,Ks,L _p		$4.49 \pm 0.05, 4.46 \pm 0.02, 4.42 \pm 0.02, 4.40 \pm 0.02$	0.05 this work ^b
		HIP 99770 b	
		Relative Astrometry	
Date	Instrument	Position [E,N]"	SNR (ADI, ASDI)
20200729	SCExAO/CHAR	IS $[0.263, -0.367] \pm [0.004, 0.005]$	5.2, 11.3
20200901	SCExAO/CHAR	IS $[0.263, -0.366] \pm [0.005, 0.005]$	7.3, 16.3
20210519	SCExAO/CHAR	IS $[0.280, -0.343] \pm [0.004, 0.004]$	17.3, 39.4
20210603	Keck/NIRC2	$[0.286, -0.337] \pm [0.006, 0.006]$	11
20210713	SCExAO/CHAR	IS $[0.286, -0.338] \pm [0.004, 0.004]$	11.7, 22.8
20211017	SCExAO/CHAR	IS $[0.292,-0.327] \pm [0.004,0.004]$	24.9, 45.0
		Photometric, Spectroscopic, and Orbital Prop	erties
$m_J (1.25 \ \mu m)$		17.39 ± 0.19	
$m_H (1.65 \ \mu m)$		16.51 ± 0.11	
m_{K_s} (2.16 μm)		15.66 ± 0.09	
$m_{L_{\rm D}} (3.78 \ \mu m)$		14.52 ± 0.12	
Spectral Type		L7-L9.5	
$T_{ m eff}$		$1400^{+200}_{-100} \mathrm{K}$	
$\log(L/L_{\odot})$		-4.55 ± 0.02	
$\log(g)$		4–5	
Mass		$16.1^{+5.4}_{-5.1}\mathrm{M_{J}}^{c}$	
Mass Ratio (q)		$0.0087^{+0.0029}_{-0.0029}$	
$a_{ m p}$		$16.9^{+3.4}_{-1.9}$ au	
e		$0.25^{+0.14}_{-0.16}$	
i		148^{+13o}_{-11}	
Predicted contrast (575nm)		$1.7 \times 10^{-10} - 2.3 \times 10^{-9}$	
Predicted contrast (660nm)		$7.9 \times 10^{-9} - 2.9 \times 10^{-8}$	
Predicted contract (720nm)		67×10-8 04×10-8	

Predicted contrast (730nm) $6.7 \times 10^{-8} - 9.4 \times 10^{-8}$ Notes - a) See Supplemental Materials. b) The star is unsaturated in 2MASS $K_{\rm s}$ band. We estimated its J, H, and $L_{\rm p}$ photometry assuming the colors of an A5V star. c) Adopting a $1/M_{\rm p}$ prior, the mass and mass ratio change to $M_{\rm p} = 13.9^{+6.1}_{-5.1}$ M_J and $q = 0.0077^{+0.0031}_{-0.0031}$.

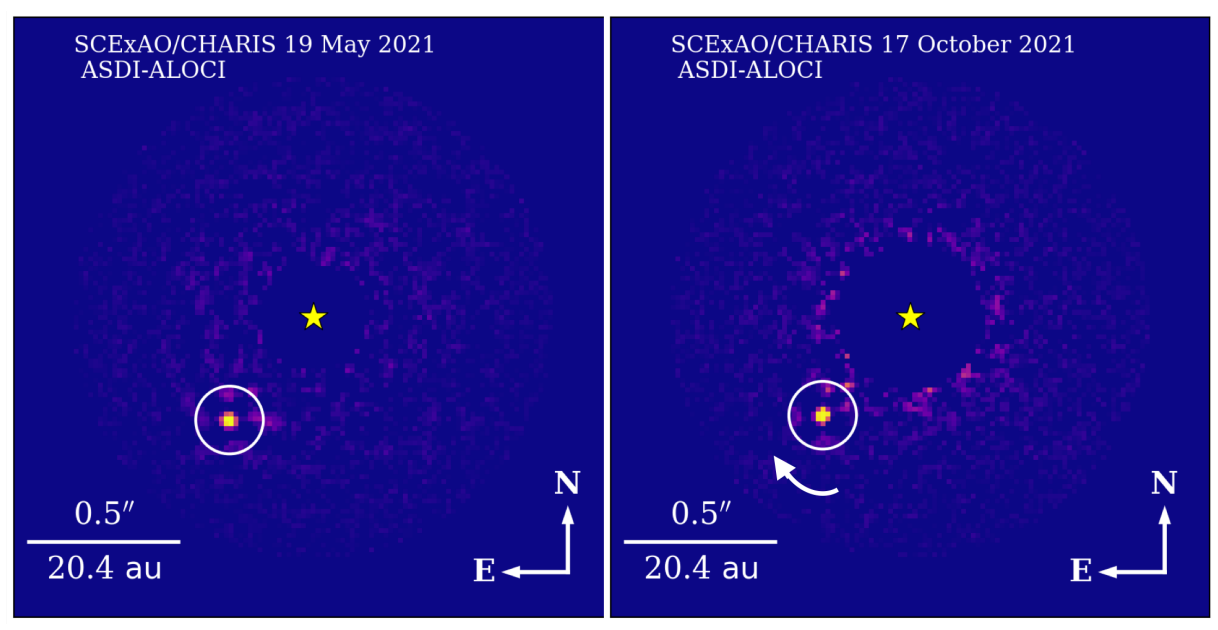


Figure 1: High signal-to-noise ratio detections of HIP 99770 b with SCExAO/CHARIS from 19 May 2021 and 17 October 2021: our two highest-quality data sets. We used the ALOCI algorithm in combination of *angular differential imaging* (ADI) and *spectral differential imaging* SDI (ASDI) to remove the stellar halo light (33–35). The curved arrow in the right panel shows the direction of HIP 99770 b's motion on the sky. The color intensity scalings are linear with a minimum of zero and maximum scaled to the mean signal within a PSF core.

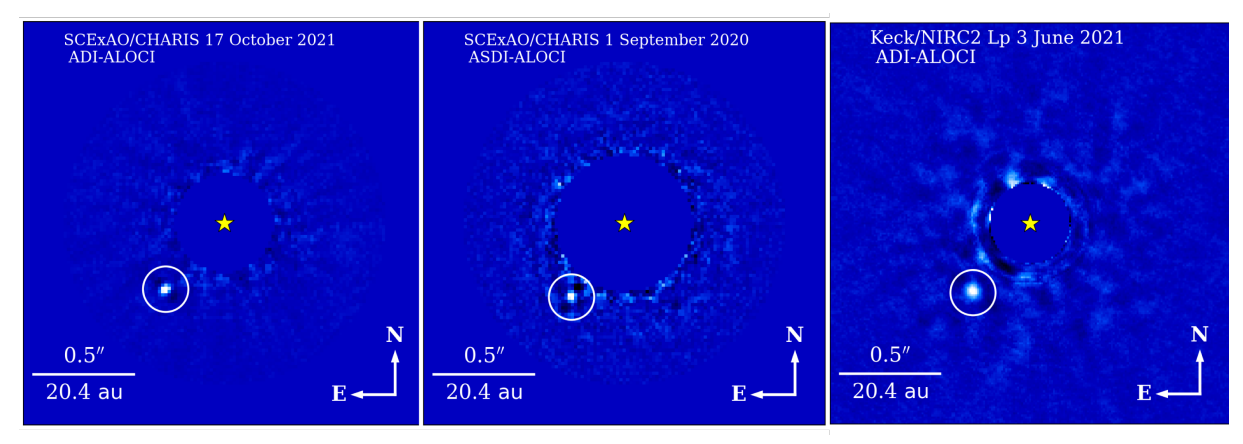


Figure 2: Additional detections of HIP 99770 b used for characterization. (left) The 17 October 2021 data reduced with ADI used to extract a robust planet spectrum. (middle) One of two HIP 99770 b detections from 2020 to lengthen the astrometric baseline. (right) Detection of HIP 99770 b from Keck/NIRC2 thermal IR imaging to extend the planet's wavelength coverage for atmospheric characterization.

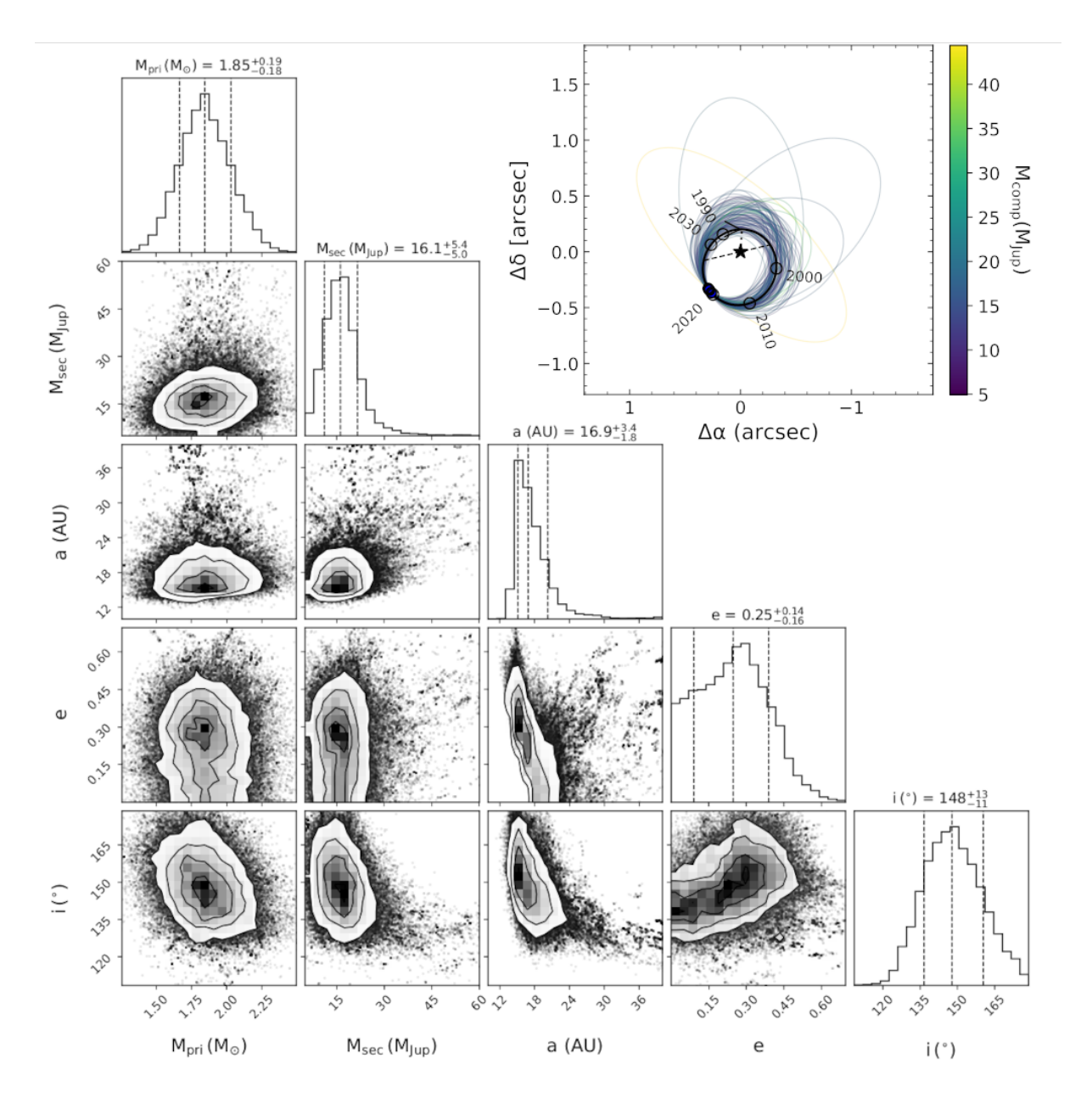


Figure 3: Corner plot showing posterior distributions of selected orbital parameters. The orbit fits used *Hipparcos* and *Gaia* absolute astrometry for HIP 99770 A and relative astrometry of HIP 99770 b. The posterior on HIP 99770 A's mass is similar to our adopted prior of $1.8 \pm 0.2~M_{\odot}$. The inset displays the best-fit orbit along with 100 orbits drawn from our MCMC posterior, color-coded by HIP 99770 b's mass.

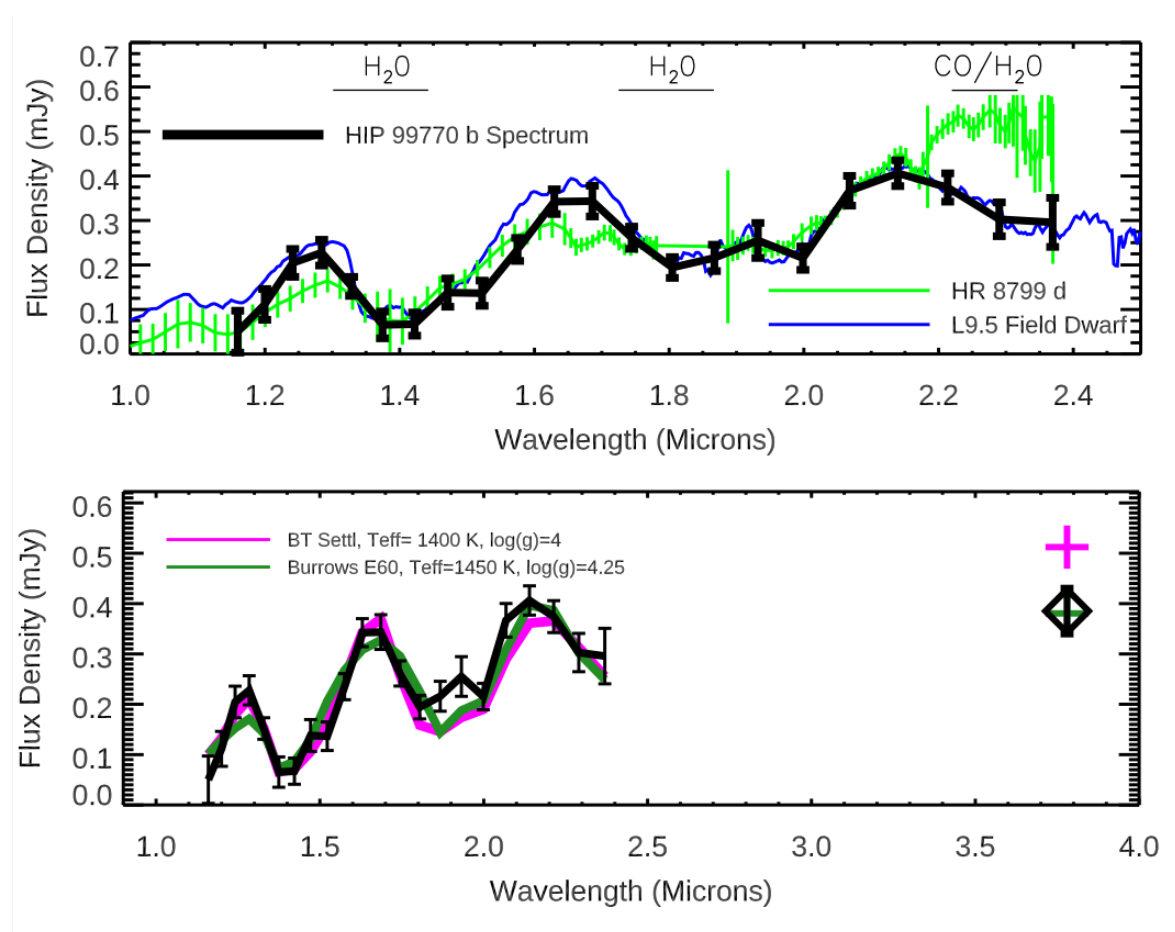


Figure 4: (top) HIP 99770 b spectrum compared to spectra for HR 8799 d extracted from GPI and SPHERE data (36,37) and the L9.5 field dwarf SIMPJ0956-1447 drawn from the Montreal Spectral Library. The HR 8799 d and SIMPJ0956-1447 spectra are normalized to HIP 99770 b's at 2.1 μm . We overplot regions of the spectrum shaped by absorption due to water and carbon monoxide. (bottom) HIP 99770 b's spectrum (black line) and photometry (black diamond) compared to representative, well-fitting atmospheric models from the BT-Settl and Burrows grids ($\chi^2_{\nu} = 1.35$ and 1.52, respectively) (38,39). The best-fit radii and implied masses are 0.92 $R_{\rm J}$, 3.3 $M_{\rm J}$ and 0.84 $R_{\rm J}$, 4.8 $M_{\rm J}$, respectively. Both models include clouds; the Burrows models include non-equilibrium carbon chemistry.

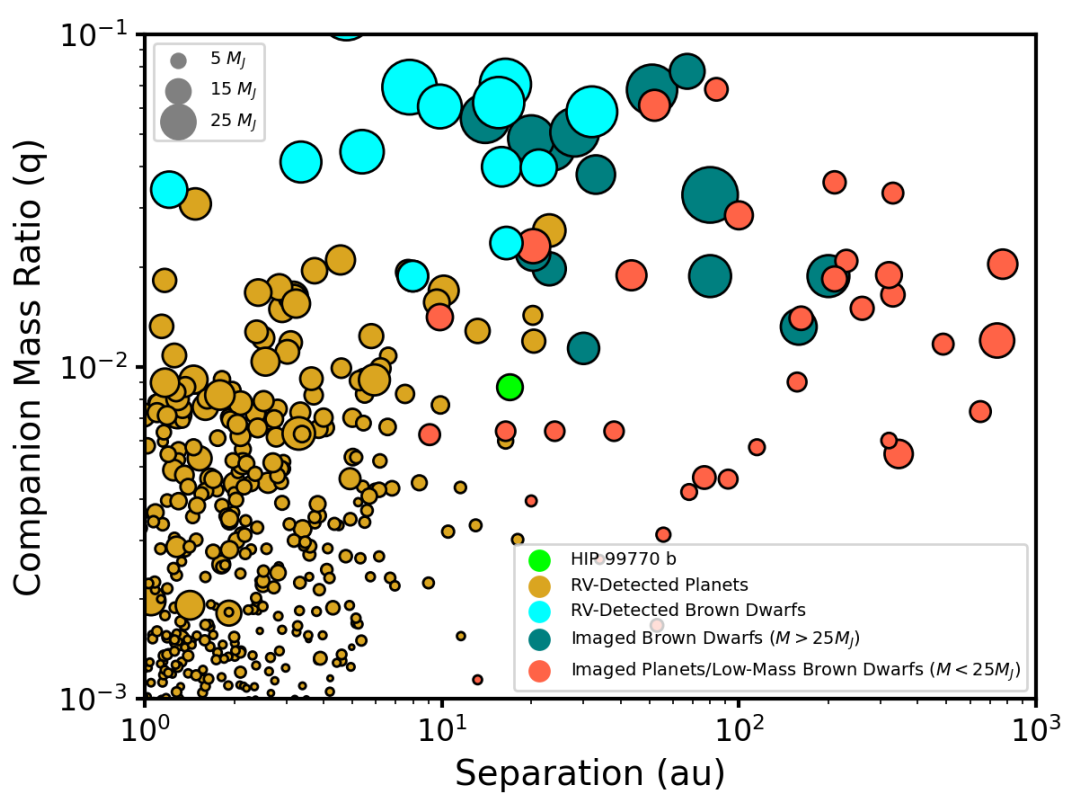


Figure 5: Mass ratio vs. separation for directly imaged exoplanets and brown dwarfs and RV-detected planets compared to HIP 99770 b. Symbol sizes are proportional to planet mass. Data are drawn from the NASA Exoplanet Archive and exoplanet.eu with small modifications. HIP 99770 b lies well within the region contiguous with RV-detected and directly-imaged exoplanets.